Molecular Biology of the Cell
Vol. 10, 197–210, January 1999

Birefringence Imaging Directly Reveals Architectural Dynamics of Filamentous Actin in Living Growth Cones[V]

Kaoru Katoh, Katherine Hammar, Peter J. S. Smith, and Rudolf Oldenbourg*

Marine Biological Laboratory, Woods Hole, Massachusetts 02543-1015

Submitted August 3, 1998; Accepted November 3, 1998
Monitoring Editor: Thomas D. Pollard

We have investigated the dynamic behavior of cytoskeletal fine structure in the lamellipodium of nerve growth cones using a new type of polarized light microscope (the Pol-Scope). Pol-Scope images display with exquisite resolution and definition birefringent fine structures, such as filaments and membranes, without having to treat the cell with exogenous dyes or fluorescent labels. Furthermore, the measured birefringence of protein fibers in the thin lamellipodial region can be interpreted in terms of the number of filaments in the bundles. We confirmed that birefringent fibers are actin-based using conventional fluorescence-labeling methods. By recording movies of time-lapsed Pol-Scope images, we analyzed the creation and dynamic composition of radial fibers, filopodia, and intrapodia in advancing growth cones. The strictly quantitative information available in time-lapsed Pol-Scope images confirms previously deduced behavior and provides new insight into the architectural dynamics of filamentous actin.

INTRODUCTION

Growth cones are specialized structures at the tip of developing neurites (Ramon y Cajal, 1909, 1995) by which nerve cells seek out target sites and form junctions with neighboring neurons and other cells. Growth cones of advancing neurites develop flat regions, called lamellipodia, that contain dense arrays of filamentous actin that is dynamically organized into cytoplasmic networks and radially aligned bundles (for recent reviews, see Heidemann, 1996; Mitchison and Cramer, 1996; Welch *et al.*, 1997). In earlier studies, the dynamic architecture of the cytoskeleton in lamellipodia was investigated with the light microscope using differential interference, phase contrast, and fluorescent-labeling techniques. The movement or retrograde flow of filamentous actin (f-actin) from the leading edge toward the central part of the cell was visualized directly either by photobleaching or by photoactivating fluorescently labeled f-actin in living fibroblasts (Wang, 1985) and other motile cells, including keratocytes (Theriot and Mitchison, 1991) and neuronal growth cones (Okabe and Hirokawa, 1991). In a series of experiments, Forscher and coworkers have used fluorescence and differential interference contrast imaging to describe retrograde flow of actin in *Aplysia* growth cones and to determine its role in growth cone motility (Forscher and Smith, 1988; Forscher *et al.*, 1992; Lin and Forscher, 1993, 1995; Lin *et al.*, 1996).

Although these imaging modes allow the investigation of dynamic aspects of cellular architecture, they have limitations that are specific to each technique. For fluorescence imaging, the cell has to be loaded with extrinsic dyes that are potentially toxic or that interfere with normal cell functions; furthermore, fluorescence is gradually bleached by multiple imaging, making the recording of long-time behavior difficult; also, fluorescence visualizes only those structures that are specifically labeled, rendering all other unlabeled components invisible. Differential interference contrast (DIC), on the other hand, does not require staining or labeling; rather it images local variations of the refractive index in the specimen. Refractive index variations are rendered into a relief-type contrast that is

[V] Online version of this article contains video material. Online version available at www.molbiolcell.org.

* Corresponding author. E-mail address: rudolfo@mbl.edu.

dependent on the mutual orientation of the refractive index gradient and the optical shear specific to DIC optics. The orientation-dependent contrast makes quantitative interpretation of DIC images difficult and usually precludes their analysis in terms of molecular organization.

Polarized light microscopy can overcome these limitations by providing fast time-lapse measurements of cellular birefringence that can be interpreted directly in terms of submicroscopic molecular order (Inoué, 1953; Inoué and Sato, 1966; Sato *et al.*, 1975; Oldenbourg, 1999). The birefringence of fibers, partially oriented filament arrays, and other ordered structures in the living cell occurs naturally, as a consequence of aligned molecular bonds and submicroscopic shapes. For example, birefringence of aligned filaments is proportional to the number of filaments in the array (Sato *et al.*, 1975; Tran *et al.*, 1995; Oldenbourg *et al.*, 1998; Oldenbourg, 1999). By measuring the birefringence, one can directly infer the density of fibers and the number of filaments in a bundle, even though the individual filaments are not resolved. Measurements can be done repeatedly, in rapid succession, documenting the dynamic behavior of cell fine structure over long periods of time without degrading image contrast or adversely affecting the cell. As an imaging device, the polarized light microscope displays the birefringence, its morphological arrangements, and its dynamic changes within the whole field of view, giving further clues as to the origin and chemical nature of molecular order. We thus can gain direct insight into the composition and dynamics of molecular organization by measuring the birefringent fine structure in living cells.

These advantages of polarized light microscopy were exploited in live cell studies that addressed specific cell structures and their functions, such as the mitotic spindle (Inoué, 1953; Salmon, 1975; Sato *et al.*, 1975; Hiramoto *et al.*, 1981; Oldenbourg, 1999), striated muscle (Taylor, 1976; Maeda, 1978), and stress fibers (Soranno and Bell, 1982). However, with the traditional polarized light microscope, one can measure birefringence retardation only in single points or areas of uniform birefringence at a time. Sequential measurements at many specimen points take an inordinately long time. Furthermore, the contrast of birefringent structures imaged in a traditional polarizing microscope is dependent not only on retardance but also on the orientation of the birefringence axis, complicating the analysis further. These shortcomings are particularly apparent in studies of motile cells that move about and that contain extended birefringent structures at several different orientations (Soranno and Bell, 1982; Ishigami *et al.*, 1987).

The shortcomings of the traditional polarizing microscope are overcome by a new type of polarized light microscope (Pol-Scope) that uses electro-optic modulators and digital image processing to measure birefringence in every image point rapidly and for all orientations of the birefringence axis simultaneously (Oldenbourg and Mei, 1995; Oldenbourg, 1996). Images recorded with the Pol-Scope represent the magnitude of specimen birefringence, independent of its axis orientation, and display the measured magnitude in shades of gray or pseudocolor. In addition to the magnitude of birefringence, the Pol-Scope also measures the orientation of the birefringence axis at each image point. Thus, Pol-Scope images display measured optical parameters that can be directly interpreted in terms of molecular organization in the specimen. Therefore, the Pol-Scope significantly enhances the analytical power of the polarized light microscope and provides orientation-independent contrast that is not available with traditional polarizing and differential interference contrast microscopes.

Using the new Pol-Scope, we have investigated the architectural dynamics of birefringent fine structures in neuronal growth cones of *Aplysia* bag cells. As tip structures that are critical in pathfinding as well as in target sensing and recognition, growth cones play an important role in the formation of the neuronal network and its connections with other cells (Letourneau *et al.*, 1991; Heidemann, 1996; McCaig, 1996). Our results include the first quantitative estimate of the number of actin filaments in radial bundles of living growth cones. Using time-lapse recordings of Pol-Scope images, we analyzed the dynamics of birefringent fine structures in the thin lamellipodial region. Our quantitative image records reveal the creation of actin bundles near the leading edge, their elongation to form filopodia and radial fibers, the continuous retrograde flow of filamentous actin toward the central domain, and the spontaneous formation and disassembly of intrapodia that are seemingly propelled by a labile and highly birefringent tail. Thus, our Pol-Scope images give new quantitative experimental results, in addition to showing more clearly what was known before or previously only deduced. The careful analysis of the quantitative information available in Pol-Scope images is leading to a more complete understanding of the architectural dynamics of living cells.

MATERIALS AND METHODS

Aplysia Bag Cell Neurons

Culture. Primary cell cultures of *Aplysia* bag cell neurons were prepared according to the methods of Kaczmarek *et al.* (1979) and Knox *et al.* (1992) and were cultured on coverslips bathed in artificial sea water. Our findings reported here are based on observations of >100 growth cones in cultures that typically were allowed to grow for 1 d. For observation in transillumination with high-resolution light microscopy, the coverslips were mounted on glass slides with thin spacers (150 μm) and then were sealed to avoid evaporation. After sealing, the preparation could be observed for several hours without visible loss of cell architecture or its dynamics.

Staining. Several growth cones were fixed with 2.5% glutaraldehyde dissolved in a solution containing 137 mM NaCl, 5 mM KCl, 2 mM $MgCl_2$, 1.1 mM Na_2HPO_4, 0.4 mM KH_2PO_4, 4 mM $NaHCO_3$, 2 mM EGTA, 750 mM sorbitol, and 5 mM piperazine-*N*,*N*′-bis(2-ethanesulfonic acid), pH 6.1 by NaOH, and were stained with rhodamine-phalloidin and with fluorescein-labeled secondary antibodies to α-tubulin, as described by Forscher and Smith (1988). After fixation, the specimens analyzed in more detail were only those that gave Pol-Scope images that were very similar to the living growth cone. For example, those fixed growth cones that showed substantially reduced birefringence of radial bundles compared with that in their living state were rejected. By observing growth cones before and after fixation with the Pol-Scope, we were able to detect even subtle fixation artifacts including loss and rearrangement of birefringent fine structure.

Polarized Light Microscopy

The design of the new Pol-Scope was reported previously (Oldenbourg and Mei, 1995; Oldenbourg, 1996). Briefly, the Pol-Scope is based on the traditional polarized light microscope, in which the crystal compensator is replaced by a universal compensator made from two liquid crystal devices (Cambridge Research and Instrumentation, Cambridge, MA; http://www.cri-inc.com). (Cambridge Research and Instrumentation also offers a commercial version of the Pol-Scope.) Electrical voltages applied to the liquid crystals control the polarization of the illuminating light that is switched between four predetermined polarization states of known ellipticities and principal axis orientations. In rapid succession, a video camera records specimen images for each of the polarization states and transfers the raw image data to a computer. On the basis of polarimetric algorithms, the raw image data are converted computationally to images representing the birefringence of the specimen in each image point, typically 640 × 480 pixels. The computed magnitude image shows all anisotropic structures, regardless of their axis orientation. As opposed to that in traditional polarized light micrographs, the contrast of birefringent fine structures in the magnitude image does not depend on the orientation of the specimen. In addition to the magnitude, the Pol-Scope software also computes the orientations of the slow birefringence axes for each image point, using the same data set of four raw images.

Birefringence expresses the difference of refractive index experienced by two orthogonally polarized light waves traversing a specimen. The Pol-Scope measures birefringence as birefringence retardation, also called retardance, that indicates the relative displacement of the two orthogonally polarized wave fronts after traversing the specimen. Hence, the retardance magnitude is given as a length in nanometers, expressing this displacement. In Pol-Scope images, retardance magnitude is typically displayed as a gray value between black and white, black indicating zero retardance and white indicating the maximum retardance displayed in the image. To enhance image contrast, pseudocolors can be used instead.

In addition to the magnitude, the Pol-Scope also measures the orientation of the slow axis of birefringence in each image point. The slow axis at a given image point corresponds to the orientation of the linear polarization of light that experiences the highest refractive index when traversing the specimen at that point.

The uncertainty of birefringence measurements in Pol-Scope images of the *Aplysia* growth cone corresponded to 0.06 nm (SD) for the retardance magnitude. The SD was derived from the noise floor in image areas without any specimen birefringence. The uncertainty of slow axis orientations is typically 2° (SD). (The SD of the slow axis orientation measured at a given image point is inversely proportional to the magnitude of retardance at that point.) The following is a list of instrument parts and settings used for the current study. We used a Nikon Microphot SA microscope equipped with an apochromat, oil-immersion condenser lens with an aperture diaphragm (maximum numerical aperture of 1.4, typically set to 1.0 [see Oldenbourg *et al.*, 1998]) and a 60×/1.4 numerical aperture plan apochromat objective lens, both selected for low-polarization aberrations (all from Nikon, Melville, NY); a mercury arc lamp followed by an Ellis light scrambler (Technical Video, Woods Hole, MA) to illuminate homogeneously the back aperture of the condenser; and a narrow bandpass interference filter (546 nm; 10 nm FWHM; Omega Optical, Brattleboro, VT) to select the green mercury line for monochromatic illumination. For the Pol-Scope setup, the liquid crystal devices from Cambridge Research and Instrumentation were placed in the transillumination path before the condenser of the microscope, and a circular analyzer was added after the objective. For the birefringence measurements, a liquid crystal-detuning parameter (swing value) of 16 nm was used.

The findings reported here are based on the recording and careful analysis of >100 time-lapse records. A time-lapse record typically lasted over 15–30 min, with data recorded at time intervals of 5–30 s. For each time point, sets of four raw image data were recorded that were subsequently used to compute specimen retardances. Raw images were recorded using a video camera (charge-coupled device camera C72 from Dage/MTI, Michigan City, IN), eight-bit analog-to-digital conversion (frame grabber AG-5 from Scion, Frederick, MD), and eight frame averaging to reduce camera-read noise. The total time elapsed during the recording of raw image data for one time point was 1.5 s. Computed retardance images were assembled into time-lapse movies that can be played back on computer or video screens using standard hardware and software.

RESULTS

Using the new Pol-Scope technique, we made time-lapse recordings of the birefringent fine structure in the growth cones of *Aplysia* bag cell neurons. A single frame of a time-lapse record representing the major structural elements is shown in Figure 1. The graph in Figure 1 illustrates the quantitative nature of image records, in which each pixel holds the retardance value measured in the specimen at that location. In the RESULTS, we introduce the major birefringent elements of lamellipodia and report their dynamic behavior. We will also present evidence that birefringent fibers in the lamellipodium stain with rhodamine-phalloidin and are therefore based on filamentous actin. In the DISCUSSION, we will consider the interpretation of the quantitative and dynamic birefringence information and discuss it in light of previous findings of actin structure and dynamics in the growth cone. In the APPENDIX, we present a more detailed analysis of the birefringent fine structure of the leading edge of the growth cone.

Birefringent Fine Structure in Lamellipodia

Growth cones of *Aplysia* bag cells form large and thin lamellipodia with a width of several times 10 μm and a thickness of only 1 μm or less near the leading edge. Because the lamellipodia are so thin, their images are unencumbered by out-of-focus information and can be analyzed directly without image restoration.

Figure 1 shows a Pol-Scope image of an *Aplysia* bag cell growth cone. Aside from the highly birefringent central domain, which contains vesicles and dense arrays of parallel fibers, the figure shows the thin, veil-like lamellar domain of the growth cone with

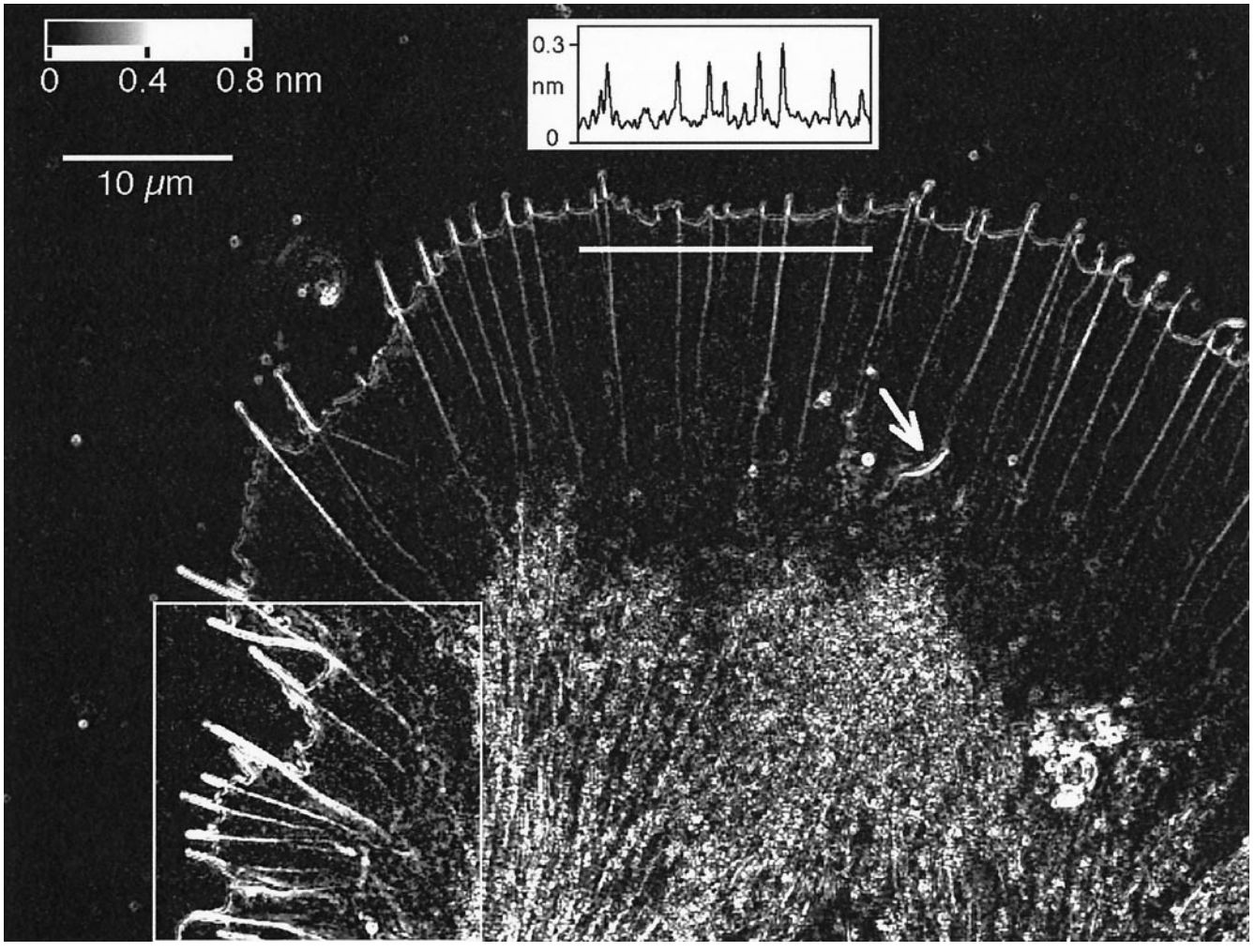

Figure 1. Birefringent fine structure in the living growth cone of an *Aplysia* bag cell neuron. This retardance magnitude image, recorded with the Pol-Scope, shows the peripheral lamellar domain containing radially aligned birefringent fibers that end in filopodia at the leading edge of the growth cone. The graph in the top center shows the retardance magnitude, in nanometers, measured along a three-pixel-wide strip that is indicated by a horizontal white bar below the graph. The measured peak retardance in radial fibers can be interpreted in terms of the number of filaments in the fibers. Near the bottom, the image shows the central domain, which is filled with vesicles and highly birefringent fibers. On the bottom left, a region is outlined, and its image contrast is enhanced to show clearly the diffuse birefringent patches located mainly in the transition region between the thin lamellar and thicker central domain. The arrow near the center of the image points to a spontaneously formed intrapodium with its strongly birefringent tail. The image is one frame of a time-lapse record that reveals the architectural dynamics of the cytoskeleton including the formation of new filopodia and radial fibers and the continuous retrograde flow of birefringent elements in the peripheral domain. The top left corner of the image contains a gray horizontal bar with the retardance scale and a 10 μm scale bar.

filopodia at the leading edge and radial fibers extending from filopodia backward to the central domain. In addition, transient birefringent patches are located between radial fibers in the lamellipodium and in the transition region between the thin lamellipodium and the thicker central domain. This transition region can also spawn highly motile intrapodia with strongly birefringent tails. In the following we briefly describe the birefringence of each of these structural elements.

Figure 2 is a highly magnified portion of a retardance image showing the birefringence of radial fibers and filopodia at the leading edge of a living growth cone. The retardance magnitude is overlaid by lines indicating the measured orientations of the slow axis of birefringence.

Radial Fibers. The birefringence of radial fibers located inside the lamellipodium typically varies between 0.15- and 0.40-nm retardance (see graph in Figure 1). The variation is caused by the varying number of filaments in the fibers (see the DISCUSSION). The slow axis of birefringence is oriented parallel to the

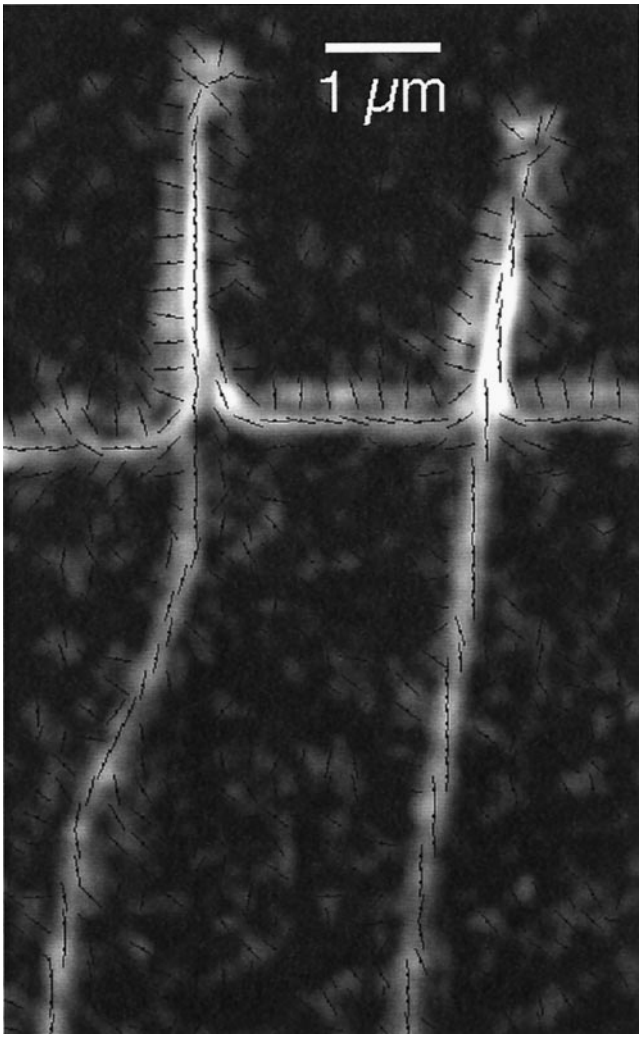

Figure 2. Radial fibers and filopodia near the leading edge recorded by the Pol-Scope (highly enlarged with digital smoothing). The retardance magnitude image is overlaid by short lines indicating the orientations of the slow birefringence axis measured in each location. The birefringence of radial fibers and the cores of filopodia have slow axis orientations that are parallel to the fiber axis. The cell membrane at the leading edge is imaged as a birefringent double layer with mutually orthogonal slow axis orientations. The double layer does not represent the lipid bilayer but is mainly caused by the refractive index difference between the optically denser cytoplasm and the surrounding medium. The slow axis of the double layer is parallel to the interface at the high-refractive index side (cytoplasm) and perpendicular to the interface at the low-refractive index side (medium) (Oldenbourg, 1991). White corresponds to 0.34-nm retardance. Slow axis orientations are typically shown for every second pixel in the horizontal and vertical direction of the original video frame. Bar, 1 μm.

fiber axis (Figure 2), in accordance with earlier findings for other protein fibers (Oldenbourg *et al.*, 1998).

Filopodia. The core birefringence of filopodia can be as high as 1-nm retardance (Figure 1) and has a slow axis orientation that is parallel to the filopodium axis (Figure 2). The core is surrounded by a second layer of birefringence that has a slow axis orientation that is perpendicular to the filopodium axis except near the tip. At the tip the second layer frequently forms a somewhat enlarged circle with slow axis directions pointing radially outward.

The Leading Edge. The leading edge is imaged as a birefringent double layer. (We use the term leading edge for the most advanced, front edge of a lamellipodium.) The two layers have birefringence axes that are oriented orthogonally to each other (Figure 2). The retardance magnitude of these layers varies with position and time, averaging 0.3 nm on the cytoplasmic side and 0.25 nm on the extracellular side. Although a convenient indicator of the location of the cell membrane, the double layer does not represent the lipid bilayer but is caused by membrane structures and by an edge effect marking the change in refractive index across the membrane. The cell membrane separates the denser cytoplasm from the outside medium that has a refractive index close to that of water. The birefringent double layer is thus, in part, caused by a steep refractive index gradient across the membrane (Oldenbourg, 1991). The same refractive index gradient is also responsible for the optical appearance and the relief effect of the cell membrane imaged by differential interference contrast microscopy (see also the APPENDIX).

Birefringent Patches. In the lamellipodium one can see birefringent patches (Figure 1) located between the radial fibers. Their birefringence is weaker than those of the radial fibers, and their slow axis tends to be oriented perpendicular to the fibers (Figure 3). These patches are more prominent in some regions of the lamellipodium than in other regions. Typically, the patches are observed behind an active, often advancing leading edge that has a dense and mobile array of filopodia and radial fibers.

Intrapodia. Spike-like, fast-moving aggregates (Figure 1) can form spontaneously in the lamellipodial region. These so-called intrapodia (Rochlin *et al.*, 1997) leave a highly birefringent tail in their wake. The slow axis orientation of the birefringence is parallel to the tail (Figure 4), consistent with the understanding that parallel fiber arrays form the tail.

Dynamics of Birefringence in Lamellipodia

In this section we will analyze some of the dynamic behavior of filopodia, radial fibers, and the birefringent elements in the growth cone that participate in retrograde flow away from the leading edge and toward the central domain. Most growth cones studied were slowly advancing at a speed of not >1 μm/min,

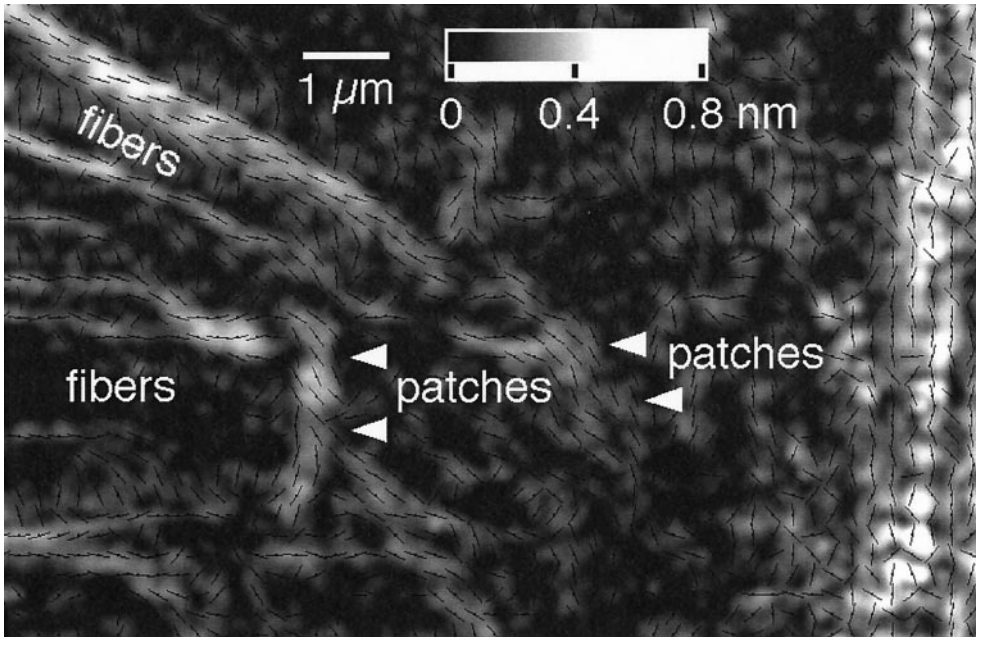

Figure 3. Birefringent patches in the transition region between the thin part of the lamellipodium (left side of the image) and the central domain of the growth cone (near the right border of the image; an enlarged portion of the framed region on the lower left of Figure 1 with slow axis overlay [see Figure 2]). Arrowheads point to some of the stronger birefringent patches that are not directly associated with radial fibers. These patches tend to be elongated in the direction perpendicular to the radial fibers, and their slow axis orientation is parallel to the elongation direction. The retardance scale is given at the top. Slow axis orientations are indicated for every second pixel. Bar, 1 μm.

which is considerably slower than the speed of retrograde flow (3.1 μm/min). (All velocities given in this article were measured in the laboratory frame of reference.) The architectural dynamics of the living growth cone is vividly demonstrated and available for quantitative analysis in two QuickTime movies accompanying this article. We also composed still-frame sequences to illustrate some of the dynamic aspects of birefringent elements of the growth cone.

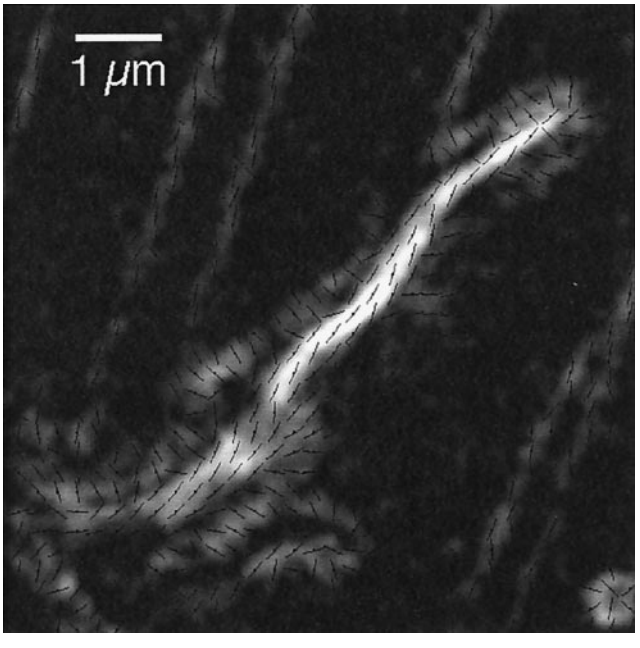

Figure 4. Spontaneously created intrapodium with its highly birefringent tail (an enlarged magnitude image with slow axis overlay [see Figure 2]). Slow axis orientations of the tail birefringence are parallel to the long axis of the tail. White corresponds to 1-nm retardance. Slow axis orientations are indicated for every second pixel. Bar, 1 μm.

Generation and Dynamics of Filopodia and Radial Fibers. Figure 5 shows the creation of new birefringent fibers and filopodia near the leading edge of the growth cone. We found that the creation of new filopodia is typically preceded by the appearance of a birefringent spot at the leading edge. The slow axis of birefringence in the spot is oriented approximately perpendicular to the edge. The spot then grows at a constant rate (1.8 ± 0.2 μm/min; mean ± SD; n = 12, where n is the number of observations) into a fiber that seems to push the filopodium out of the leading edge. The slow axis of the central part of the filopodial birefringence is parallel to the long axis of the fiber inside; hence it has the same orientation as the spot birefringence. New filopodia are often tilted with an angle of 60 ± 8° (n = 16) to the leading edge. We have observed that some regions of the leading edge generate more new filopodia than other regions. Those highly productive regions tend to launch filopodia in regular time intervals and in the same direction with the same tilt angel (Movies 1 and 2). In their early stage, most newly formed filopodia have no detectable birefringent fibers in the peripheral lamellar region near the edge.

After the birefringent fiber and filopodium extend forward, a radial fiber appears and elongates in the lamellipodium toward the center of the growth cone.

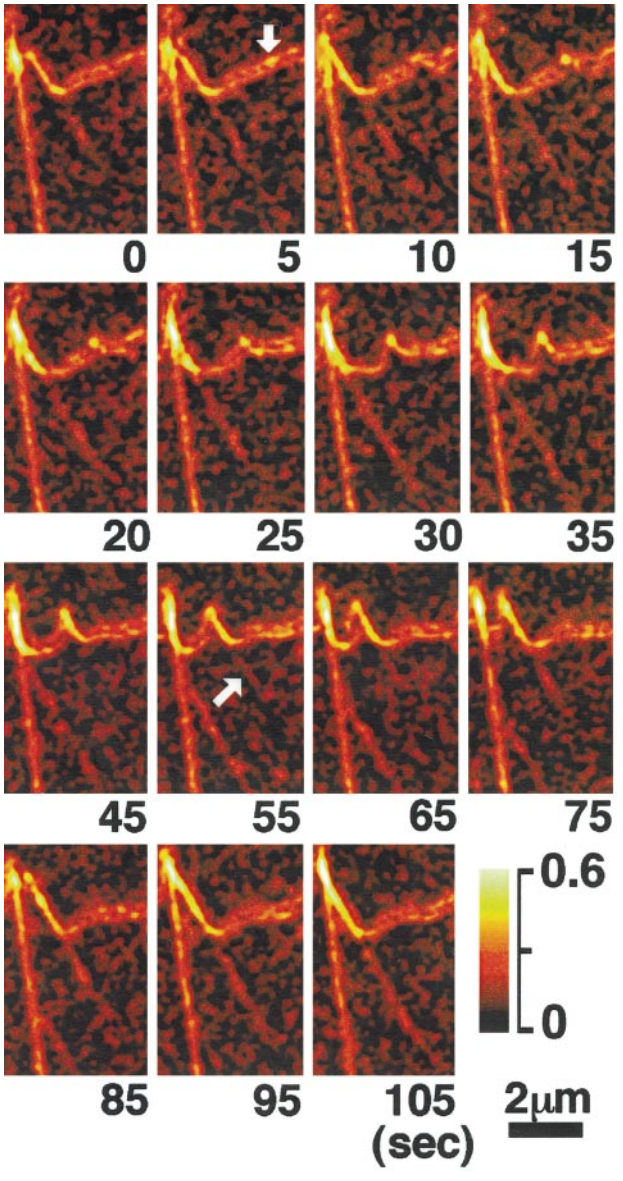

Figure 5. Magnified time-lapse record showing the creation of a birefringent fiber and filopodium. The retardance magnitude is in pseudocolor; the numbers below each record give the time in seconds elapsed since the first record. The formation of the filopodium is preceded by the appearance of a birefringent spot at the leading edge of the growth cone (arrow in the 5-sec record). The spot elongates into a filopodium and generates a visible actin bundle (arrow in the 55-sec record) that extends toward the center of the lamellipodial region. The newly formed filopodium and fiber are tilted to one side, move laterally, and fuse with a neighboring, stable filopodium (85- to 105-sec records). In the 5- to 95-sec records, the same stable filopodium is seen to fuse with another filopodium and fiber, generated earlier. Lower right, pseudocolor retardance scale in nanometers. Bar, 2 μm.

Near the leading edge, the rate of elongation (6.1 $\pm$ 1.0 μm/min; n = 12) of the detected end point of the birefringent radial fiber is about three times the rate of elongation of a new filopodium. After the fiber has grown >1 μm long into the lamellipodium, its rate of elongation reduces to the speed of retrograde flow that is also exhibited by other birefringent fine structures in the region.

Tilted filopodia and fibers move laterally, sometimes crossing over several neighboring filopodia and fibers (Movies 1 and 2). A few of the new filopodia eventually change their angle to lie parallel to neighboring filopodia, stop their lateral travel, and become stable filopodia themselves. Stable filopodia, in turn, can become unstable; they can start to tilt with respect to the leading edge and to travel laterally. The majority of tilted, traveling filopodia fuse with one of their more stable neighbors (Figure 5). The fusion starts at the tip of the traveling filopodium where it forms a branching point with its stable neighbor. As the fusion progresses, the branching point moves down the length of the filopodia and then that of the radial fibers in the lamellipodial region. The birefringence of the fused fiber, when measured immediately after the fusion process, is approximately the sum of the individual fibers, suggesting that the number of filaments in the fused fiber is the sum of the filaments in each fiber. In some cases, a transient apical elongation of a stable filopodium occurs after it fuses with a neighbor (Movies 1 and 2). The elongation over a few micrometers often lasts for ~1 min, at which point the filopodium returns to its initial length. In some fusion events, a region of high birefringence in the fused bundle appears to "separate" from the leading edge and, without changing its length, to slide down along the radial fiber bundle (Figure 6). This observation suggests that one of the fused fibers detaches from the leading edge and slides down the remaining fiber toward the central domain.

Retrograde Flow. The sliding fiber and the branching point of fusing fibers are two transient elements of the birefringent fine structure in the peripheral domain of the growth cone that exhibit retrograde movement from the leading edge back to the central domain (Figures 5 and 6). We found other structural elements that exhibit retrograde flow, including kinks or birefringent swirls that occur spontaneously in radial fibers. The weak but discernible patches of birefringence (Figures 1 and 3), which fill the space between radial fibers, also participate in retrograde flow. All these structural elements move toward the center of the growth cone at the same average speed of 3.1 $\pm$ 0.5 μm/min (n = 20), which is independent of the rate of advance of the leading edge. The retrograde flow of birefringent structural elements is vividly displayed in Movies 1 and 2.

Intrapodia. In many growth cones, we observed highly motile objects that formed spontaneously and were seemingly propelled by a highly birefringent tail

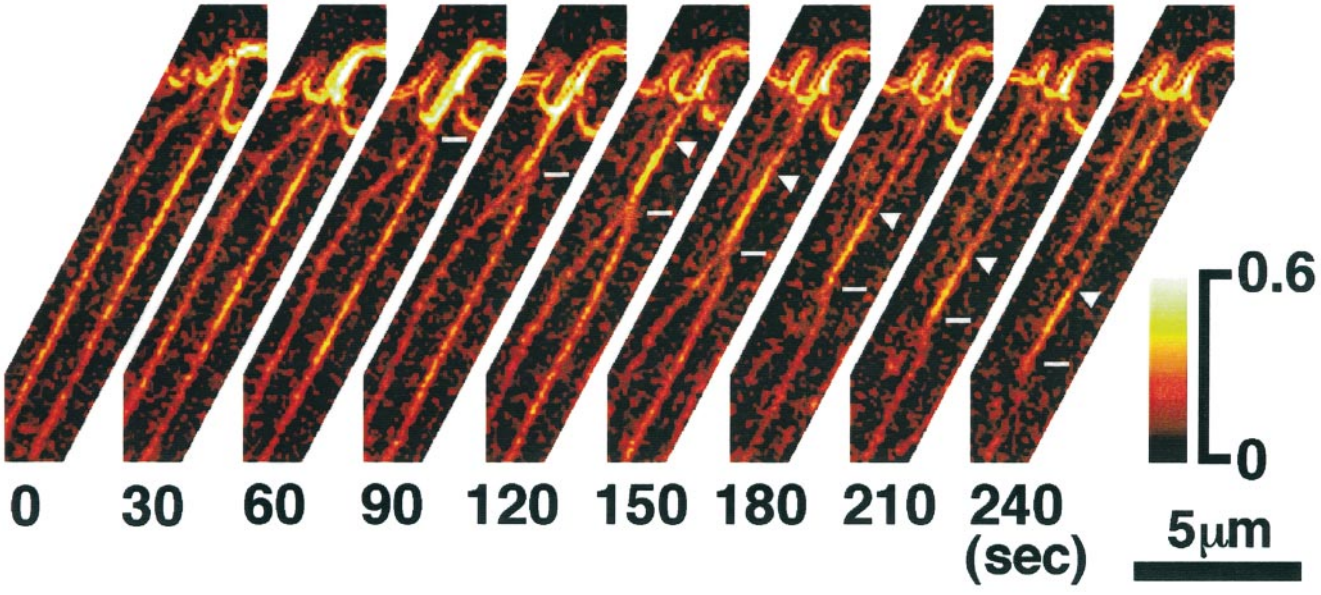

Figure 6. Magnified time-lapse record of the lateral fusion of radial fibers and of the relative motion of fused fibers. The retardance magnitude is in pseudocolor; the numbers below each record give the time in seconds elapsed since the first record. Two neighboring radial fibers fuse, starting at the leading edge and proceeding down toward the central domain (horizontal line marker in the 60- to 240-sec records). In the 120-sec record, the high-birefringent region of the fused fiber separated from the leading edge (arrowhead in the 120- to 240-sec records) and moved down the stable fiber toward the central domain at a speed of 3.0 ± 0.2 μm/min, which is the same as retrograde flow. Lower right, pseudocolor retardance scale in nanometers. Bar, 5 μm.

(Figures 1 and 4 and Movie 1). Recently, these spontaneously formed structures were labeled intrapodia (Rochlin *et al.*, 1997). They resemble the actin-rich structures induced by intracellular pathogens (e.g., *Listeria* [Dabiri *et al.*, 1990; Sanger *et al.*, 1992; Theriot *et al.*, 1992]) or by extracellular polycation-coated beads (inductopodia [Forscher *et al.*, 1992]). Our time-lapse records demonstrate that one end of the tail remains almost stationary, whereas the other end moves with high speed (8.31 + 1.56 μm/min; n = 11) on a seemingly random path. After the tail is formed, it does participate in retrograde flow and moves to the transition region near the central domain where it is seemingly disassembled, like other f-actin–based structures, and disappears.

Birefringence of f-Actin–Stained Structures

To ascertain which of the birefringent fine structures in the peripheral domain of the growth cone are based on filamentous actin, we fixed *Aplysia* bag cells, labeled them with rhodamine-phalloidin, and imaged them with fluorescence microscopy, with the Pol-Scope, and, for comparison, with DIC microscopy. Figure 7 shows a growth cone shortly before and after fixation, both times imaged with the Pol-Scope and DIC. The fixed growth cone was double labeled with rhodamine-phalloidin and fluorescein-tagged secondary antibodies to α-tubulin to show the distribution of microtubules that were found concentrated in the central region of the growth cone. Rhodamine-phalloidin stains the f-actin–rich peripheral domain with radially

Figure 7 (facing page). Growth cone of an *Aplysia* bag cell neuron that was fixed, double-labeled for f-actin and microtubules, and imaged with the Pol-Scope, with differential interference contrast, and with fluorescence microscopy. (A) Retardance magnitude image of living growth cone shortly before fixation, imaged with the Pol-Scope. (B) Living growth cone imaged by DIC. (C) Fixed growth cone imaged with the Pol-Scope. (D) Fixed growth cone in DIC (bias retardance inverted compared with that in B). (E) Rhodamine-phalloidin stain in fixed growth cone indicating the distribution of filamentous actin. (F) Fluorescein-tagged tubulin secondary antibody indicating the distribution of microtubules in the fixed growth cone. (G and H) Magnified rhodamine fluorescence and Pol-Scope images, respectively, of the same area in the peripheral lamellar domain near the leading edge. The fluorescence images reveal the radial birefringent fibers and the weakly birefringent areas between fibers in the peripheral domain as f-actin based, whereas the birefringence in the central domain is attributable in large part to microtubules that are absent from the peripheral domain. Note in the DIC images the orientation-dependent contrast of radial fibers because of optical shear, whereas contrast variation in the Pol-Scope images of radial fibers is caused by the variation in the number of actin filaments in the bundles. In birefringence images, a retardance of 0.8 nm, or higher, is displayed as white. Bars: A–F, 10 μm; G and H, 2 μm.

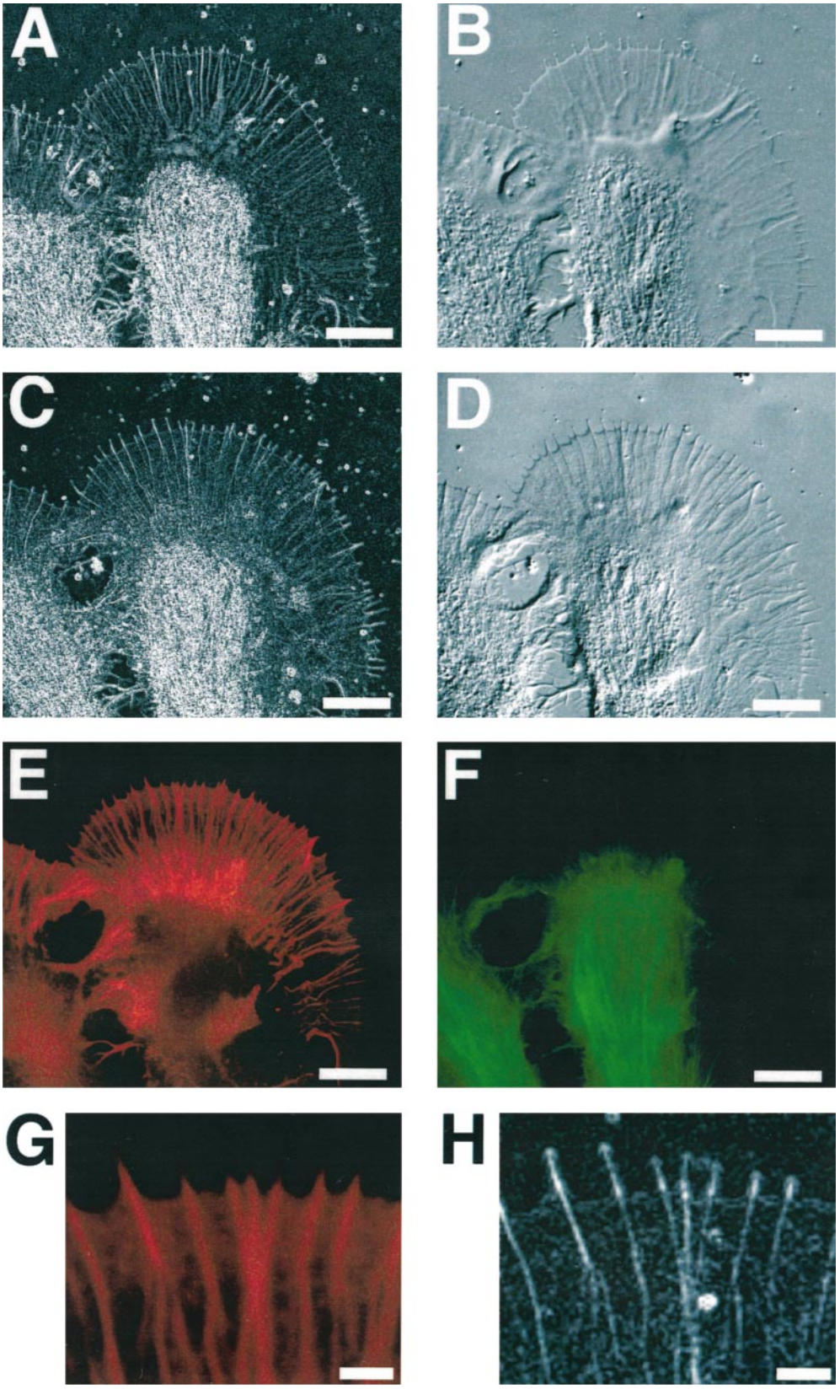

Figure 7.

aligned actin bundles. A close examination of birefringence and fluorescence images of the peripheral, actin-rich region reveals that radial actin bundles in the fluorescence images were identical to the radial birefringent fibers in Pol-Scope images.

The space-filling network of actin filaments in the lamellipodium appears as a continuous rhodamine stain between the radial bundles. In the birefringence images, the actin network causes an increased retardance magnitude recorded as birefringent patches located between radial bundles. Both the magnitude of retardance and the density of the continuous fluorescence increase toward the thicker portion of the lamellipodium near the central domain (Figure 7, C and E). However, the increase in fluorescence considerably exceeds the increase in retardance magnitude, indicating that actin filaments in the thicker, more densely packed transition region lack preferential orientation. In fact, the measured slow axis orientation of the weak birefringent patches between radial actin bundles in the lamellipodium of fixed growth cones varies randomly over short distances, whereas the slow axis orientation in the living growth cone is more homogeneous, corresponding to the larger birefringence patches observed in the living growth cone. Although birefringence patches in the fixed growth cone are distinctly smaller in size, their average retardance magnitude is higher than that in the living growth cone (compare brightness levels of corresponding regions in Figure 7, A and C).

As additional observations, we note that the front edge of the lamellipodium shows no elevated rhodamine-phalloidin staining. This indicates that there is no enhanced concentration of actin filaments at the front edge, supporting the interpretation that the birefringent double layer at the front edge is caused mainly by edge birefringence. Furthermore, the actin bundles inside filopodia stain only weakly with rhodamine-phalloidin, compared with the increased retardance magnitude of filopodia.

DISCUSSION

Birefringence in the Peripheral Domain Is Mostly Actin-based

The fluorescence images in Figure 7 show the f-actin–rich peripheral domain with radially aligned actin bundles and the microtubule-rich central domain with little actin-based structures, as reported previously (Yamada *et al.*, 1971; Tosney and Wessells, 1983; Forscher and Smith, 1988; Bridgman and Dailey, 1989). The transition region between the lamellar and central domain contains both f-actin and microtubules and seems to provide a zone of enhanced interaction between the two filament networks populating each domain. The weak birefringence located between radial fibers in the thin lamellipodial region is distinctly different in its organization between the living and fixed growth cone. Under the likely assumption that this birefringence can be attributed in both specimens to the actin network (rather than to membrane, membrane remnants, or cytoskeletal structures other than actin), the difference in birefringent fine structure can be interpreted in terms of the difference in network organization. It then seems likely upon fixation that the homogeneous actin network in the living cell is disrupted and collapses in the fixed cell into a more heterogeneous network with smaller regions of more highly ordered filaments.

In an earlier study, we reported the elimination of all dynamic birefringent elements in lamellipodia of living growth cones by treating them with cytochalasin B (Katoh *et al.*, 1997). This is further evidence that the dynamic birefringent structures such as radial fibers and birefringent patches between fibers are indeed f-actin based (Yamada *et al.*, 1970; Forscher and Smith, 1988).

Birefringent Fine Structure in Lamellipodia

Radial Fibers. The birefringence of a radial fiber in the lamellipodium has its slow axis oriented parallel to the fiber axis. This anisotropy of protein fibers is caused primarily by form birefringence, which results in the slow axis being parallel to the fiber axis (Oldenbourg *et al.*, 1998). The radial fibers in the growth cone are composed of actin filaments bundled together by actin-associated proteins. For small protein bundles, the measured retardance magnitude increases linearly with the number of filaments in the bundle (Tran *et al.*, 1995; Oldenbourg *et al.*, 1998). Using previous measurements of the birefringence of the acrosomal process of *Limulus* sperm, we found that a single actin filament, including actin-associated proteins, has a retardance of 0.01 ± 0.001 nm (Katoh *et al.*, 1996). Therefore, using the retardance range of 0.15–0.40 nm for stable radial fibers, we estimate that those fibers in the growth cone of *Aplysia* bag cell neurons are composed of between 15 and 40 actin filaments. The same range of actin filaments per bundle was observed in growth cones by electron microscopy (Bridgman and Dailey, 1989; Lewis and Bridgman, 1992; Heidemann, 1996).

Our analysis of f-actin dynamics in the lamellipodium is based in part on the unique capability of the Pol-Scope to measure the number of filaments in bundles dynamically, all along the length of the bundles, and over the whole lamellipodium simultaneously.

Filopodia. Filopodia formation is preceded by the appearance of a birefringent spot, typically located in the outer layer of the leading edge birefringence (Figure

5). The spot grows into a fiber that seems to push the filopodium out of the leading edge. On the basis of electron microscopy studies (Yamada *et al.*, 1971; Lewis and Bridgman, 1992), filopodia are composed of a central actin bundle wrapped by a sheet of cell membrane material. Thus, filopodia birefringence is a composite of fiber birefringence and the birefringence attributable to membrane structures.

The core or peak retardance of filopodia has typically twice the magnitude of the associated radial fibers seen in the lamellipodium. This enhanced core retardance of filopodia arises from several contributions. In a recent study on microtubule birefringence, we have shown that the peak retardance of a thin fiber is proportional to the mass per unit length of the fiber. Thus, the increased core retardance of filopodia is probably caused by the increase in mass because of the membrane sheet. Adding to the mass per unit length might be an increased number of actin filaments in the filopodia core, because of f-actin promoters in the membrane (Izzard, 1988; Welnhofer *et al.*, 1997). Finally, filopodia birefringence is enhanced because they are surrounded by medium that has a lower refractive index compared with that in the cytoplasm that surrounds radial fibers (see the APPENDIX).

The second layer of birefringence surrounding the core is caused primarily by diffraction, similar to the subsidiary maxima of axonym images recorded with the Pol-Scope (Oldenbourg *et al.*, 1998).

Although the birefringence of the filopodia is increased with respect to their associated radial fibers in the lamellipodium, we found that the fluorescence caused by rhodamine-phalloidin staining is noticeably reduced in the filopodia. This might in part be caused by a reduced affinity of the phalloidin stain to f-actin inside filopodia because of the competing binding of actin-associated proteins located in the former cell membrane.

The Leading Edge. The fluorescent-staining experiments have shown that the leading edge of the fixed growth cone does not have an elevated concentration of filamentous actin (Figure 7). What else contributes then to the birefringent double layer observed near the leading edge?

Although edge birefringence is an important contributor to the birefringent double layer, it is probably not the sole cause of the measured birefringent fine structure at the leading edge (see the APPENDIX). This statement is supported by several observations including the ratio of retardances measured on the cytoplasmic and extracellular side ($0.3/0.25 = 1.2$), which is significantly smaller than that for a pure refractive index step ($0.029/0.015 = 1.9$; see the APPENDIX). Furthermore, the temporal and spatial variations in the retardance magnitude of the double layer make this ratio even less than one at some locations and for some instances in time. It is therefore likely that specific structures near or in the cell membrane contribute to the measured retardance distribution. The slow axis of these additional contributions seems to be oriented preferentially perpendicular to the edge, because the layer with the perpendicular slow axis orientation shows a higher than expected retardance value. In fact, contributions from the lipid bilayer itself and from membrane proteins that have, for example, α-helices spanning the membrane are expected to have slow axis orientations that are perpendicular to the leading edge. Apparently, these structures are highly dynamic and can contribute to the organization of birefringence beyond the leading edge, as exemplified by the birefringent spot preceding filopodia formation.

Birefringent Patches. The space between radial fibers and the transition region toward the central domain shows transient patches of weak birefringence (Figures 1 and 3). The patches disappear when the cell is treated with cytochalasin B and reappear when this inhibitor of actin polymerization is washed out of the medium (Katoh *et al.*, 1997). Therefore, we interpret the birefringence in these patches as attributable to the extended actin network, which becomes partially aligned by internal stress and strain. The actin network at rest is composed of filaments that, as a whole, have no or little preferential alignment, and hence the network is not birefringent. In the process of retrograde flow, which involves actively moving the network, it is likely to be distorted, introducing stress birefringence. It seems that network distortions are compatible with all proposed models of molecular mechanisms inducing leading edge advance and retrograde flow (Mitchison and Kirschner, 1988; Smith, 1988; Heidemann *et al.*, 1991; Heidemann, 1996; Mitchison and Cramer, 1996; Welch *et al.*, 1997).

Dynamics of Birefringence in Lamellipodia

Retrograde Flow. The speed of retrograde flow of birefringent fine structure in the lamellipodium is very similar to the speed of retrograde flow in *Aplysia* bag cell growth cones reported when using markers in fluorescence and differential interference contrast microscopy (Forscher and Smith, 1988; Smith, 1988). With the same methods, retrograde flow has been observed in the lamellipodia of other motile cells (Bray and White, 1988; Heath and Holifield, 1991). Retrograde flow involves the treadmilling of actin (Theriot and Mitchison, 1991; Small, 1994) and also includes the active translocation of the actin network by motor proteins such as myosin (Lin *et al.*, 1996). Treadmilling describes the well-established phenomenon of actin filaments that add actin monomers to their plus ends

(the barbed ends that are found adjacent to attachment points to the cell membrane) and subtract them from their minus ends (generally pointing toward the center of the cell) (Wang, 1985). In the growth cone, treadmilling contributes to the constant flux of polymerized actin away from the leading edge toward the central domain.

Time-lapsed Pol-Scope images (Movies 1 and 2) demonstrate the frequent fusion and sliding of actin bundles, also described in Figures 5 and 6. The sliding of one actin bundle down another bundle might in fact be caused by treadmilling and a difference in the polymerization state of the two plus ends of the bundles; one bundle adds actin subunits to its plus end near the leading edge and therefore remains a stable radial fiber, whereas the other bundle separates from the leading edge and looses its ability to add actin monomers to its plus end. Thus, this second bundle moves down the stable bundle, driven by the constant retrograde flux of actin subunits in the stable bundle. As an alternative, actin fibers might glide relative to others based on the action of motor proteins, such as myosin, which is known to be present in the lamellipodium and the leading edge of the growth cone (Bridgman and Dailey, 1989; Wang *et al.*, 1996).

Generation of Filopodia and Radial Actin Bundles. We observed the generation of filopodia that is typically preceded by the appearance of a birefringent spot at the leading edge. The birefringent spot suggests that filopodia formation is preceded by the formation of an ordered array of molecular aggregates near the leading edge. The molecular aggregates might be a mixture of actin-associated molecules, such as f-actin promoters, and short actin filaments that then elongate and push the filopodia out the leading edge. As early as 1958, Asakura and Oosawa (1958) suggested that the polymerization of actin is composed of two steps, first the formation of short fragments and then the addition of actin subunits to the fragments.

It is interesting to note that the extension of actin filaments is first directed outward, leading to the formation of a filopodium. The initial extension of a filopodium might be the concerted effect of f-actin–nucleating sites and –bundling proteins (e.g., talin and α-actinin), both located in the cell membrane at the leading edge. A cluster of nucleating sites leads to the rapid formation of small actin filaments that bundle together and thereby pull in more membrane, leading to the extension of the filopodium. Only after the filopodium has reached a certain length does the polymerization of actin lead to extending the bundle into the lamellipodial region. The growth of radial actin bundles into the lamellipodium possibly involves two mechanisms. 1) The thick actin bundle, which forms in the core of a filopodium, is transported back to the central domain by retrograde flow, whereas its polymerization continues near the tip. 2) The early extension of radial bundles into the lamellipodium might also involve the recruitment of pre-existing actin filaments into the bundle by a zipper-like action mediated by actin-bundling proteins. This second mechanism is suggested by our observation that near the leading edge in a narrow zone of ~1-μm width, the speed of elongation of the detected end point of a radial bundle exceeds the speed of retrograde flow. When the detectable bundle end point has grown beyond the narrow zone, however, it slows down and moves toward the central domain with the speed of retrograde flow. Subsequently, all structural features in a bundle, like kinks or stretches of increased birefringence, move from the leading edge toward the central domain with the speed of retrograde flow.

Comparison between the Growth Cone Dynamics by Pol-Scope and that by Conventional DIC or Fluorescence Microscopy

In this manuscript, we describe the dynamics of actin-based structures inside living growth cones on the basis of observations made with a newly developed microscope, the Pol-Scope. Although some aspects of growth cone dynamics have been reported previously, based on fluorescence or electron microscopy of labeled or fixed samples or on DIC microscopy of living cells with limited image clarity and less quantitative image information (Goldberg and Burmeister, 1986; Forscher and Smith, 1988; Davis *et al.*, 1992; Welnhofer *et al.*, 1997), our study has directly demonstrated the dynamics of actin-based structures in living, unstained growth cones. Furthermore, the new method was able to provide quantitative interpretation of molecular organization in the actin bundles. Because birefringence is an optical property of the samples themselves (in this case, the aligned actin filaments), the imaging method using optical anisotropy (birefringence) can unveil mechanisms and behaviors of the dynamic molecular structure noninvasively in living cells. The Pol-Scope also provides exceptionally clear, highly resolved images of cell regions exhibiting birefringence.

APPENDIX

Interpreting the Birefringent Fine Structure of the Leading Edge

The birefringence of the leading edge of living growth cones is caused in part by edge birefringence. Edge birefringence is a general optical phenomenon first recognized by Inoué (1959) and recently analyzed by us using thin flakes of optically isotropic potassium chloride crystals (Oldenbourg, 1991). According to this analysis, edge birefringence around the perimeter

of thin crystal flakes increases linearly with the difference in refractive index between the crystal and the surrounding medium and with the vertical thickness of the crystal. The specific retardance of the double layer, i.e., the retardance per thickness of the crystal flake and per refractive index difference to the medium, is 0.029 on the high-index side and 0.015 on the low-index side of the steep-refractive index gradient.

The double layer at the leading edge of growth cones has the typical features of edge birefringence, including the 90° turn of the slow axis orientation from parallel to the edge on the high-refractive index side to perpendicular to the edge on the low-index side (Figure 2). The ratio of retardances measured on the cytoplasmic and extracellular side (0.3/0.25 = 1.2), however, is significantly smaller than that for a pure refractive index step (ratio of specific retardances, 0.029/0.015 = 1.9). The deviation can result from several different possibilities, including the shape of the edge differing from a simple step. Another, more interesting possibility is based on contributions to the birefringent double layer from specific birefringent structures inside or near the plasma membrane (see the DISCUSSION).

Finally, we can estimate the refractive index difference between the cytoplasm and the medium, using the measured average retardance of 0.3 nm (cytoplasmic side) and, as a rough estimate, a cell thickness of 500 nm at the leading edge of the growth cone. By dividing the measured average retardance (0.3 nm) by the specific retardance (0.029) and the cell thickness (500 nm), we obtain a refractive index difference of 0.02 between cytoplasm and medium. This estimate compares well with the refractive index difference of 0.02 derived from measurements of the cytoplasm index of living cells measured in echinoderm eggs (1.36 [Sato *et al.*, 1975; Hiramoto *et al.*, 1981]) and the refractive index of artificial sea water that is close to 1.34.

ACKNOWLEDGMENTS

We are grateful to Shinya Inoué of the Marine Biological Laboratory for his invaluable suggestions and encouragement during the course of this work and for his critical reading of the manuscript. We thank George Langford and Ana DePina of Dartmouth College in Hanover, NH, for advice in the fluorescence-labeling experiments and Colin S. Izzard of the State University of New York in Albany, NY, for very helpful discussions on actin dynamics in the growth cone. This research was supported by the BioCurrent Research Center, which is supported by the National Institutes of Health grant P41RR-01395. This work was funded by the National Institutes of Health grant GM-49210 awarded to R.O.

REFERENCES

Asakura, S., and Oosawa, F. (1958). Interaction between particles suspended in solutions of macromolecules. J. Polymer Sci. *33*, 183–192.

Bray, D., and White, J.G. (1988). Cortical flow in animal cells. Science *239*, 883–888.

Bridgman, P.C., and Dailey, M.E. (1989). The organization of myosin and actin in rapid frozen nerve growth cones. J. Cell Biol. *108*, 95–109.

Dabiri, G.A., Sanger, J.M., Portnoy, D.A., and Southwick, F.S. (1990). *Listeria monocytogenes* moves rapidly through the host-cell cytoplasm by inducing directional actin assembly. Proc. Natl. Acad. Sci. USA *87*, 6068–6072.

Davis, L., Rehder, V., and Kater, S.B. (1992). Autonomous activities of the neuronal growth cone. In: The Nerve Growth Cone, ed. P.C. Letourneau, S.B. Kater, and E.R. Macagno, New York: Raven Press, 133–149.

Forscher, P., Lin, C.H., and Thompson, C. (1992). Novel form of growth cone motility involving site-directed actin filament assembly. Nature *357*, 515–518.

Forscher, P., and Smith, S.J. (1988). Actions of cytochalasins on the organization of actin filaments and microtubules in a neuronal growth cone. J. Cell Biol. *107*, 1505–1516.

Goldberg, D.J., and Burmeister, D.W. (1986). Stages in axon formation: observation of growth of *Aplysia* axons in culture using video-enhanced contrast-differential interference contrast microscopy. J. Cell Biol. *103*, 1921–1931.

Heath, J.P., and Holifield, B.F. (1991). Cell locomotion: new research tests old idea on membrane and cytoskeletal flow. Cell Motil. Cytoskeleton *18*, 245–257.

Heidemann, S.R., Lamoureux, P., and Buxbaum, R.E. (1991). On the cytomechanics and fluid dynamics of the growth cone motility. J. Cell Sci. Suppl. *15*, 35–44.

Heidemann, S.R. (1996). Cytoplasmic mechanism of axonal and dendritic growth in neuron. Int. Rev. Cytol. *165*, 235–296.

Hiramoto, Y., Hamaguchi, Y., Shôji, Y., Schroeder, T.E., Shimoda, S., and Nakamura, S. (1981). Quantitative studies on the polarization optical properties of living cells. II. The role of microtubules in birefringence of the spindle of the sea urchin egg. J. Cell Biol. *89*, 121–130.

Inoué, S. (1953). Polarization optical studies of the mitotic spindle. I. The demonstration of spindle fibers in living cells. Chromosoma *5*, 487–500.

Inoué, S. (1959). Problems in polarization microscopy. J. Opt. Soc. Am. *49*, 508.

Inoué, S., and Sato, H. (1966). DNA arrangement in living sperm. In: Molecular Architecture in Cell Physiology, ed. T. Hayashi and A.G. Szent-Gyorgyi, Englewood Cliffs, NJ: Prentice Hall, 209–248.

Ishigami, M., Kuroda, K., and Hatano, S. (1987). Dynamic aspect of the contractile system in *Physarum plasmodium*. III. Cyclic contraction-relaxation of the plasmodial fragment in accordance with the generation-degeneration of cytoplasmic actomyosin fibrils. J. Cell Biol. *105*, 381–386.

Izzard, C.S. (1988). A precursor of the focal contact in cultured fibroblast. Cell Motil. Cytoskeleton *10*, 137–142.

Kaczmarek, L.K., Finbow, M., Revel, J.P., and Strumwasser, F. (1979). The morphology and coupling of *Aplysia* bag cell within the abdominal ganglion and in cell culture. J. Neurobiol. *10*, 535–550.

Katoh, K., Langford, G., Hammar, K., Smith, P.J.S., and Oldenbourg, R. (1997). Actin bundles in neuronal growth cone observed with the Pol-Scope. Biol. Bull. *193*, 219–220.

Katoh, K., Yamada, K., Oosawa, F., and Oldenbourg, R. (1996). Birefringence measurements of the actin bundle in *Limulus* sperm acrosomal processes. Biol. Bull. *191*, 270–271.

Knox, R.J., Quattrocki, E.A., Connor, J.A., and Kaczmarek, L.K. (1992). Recruitment of Ca^{2+} channels by protein kinase C during rapid formation of putative neuropeptide release site in isolated *Aplysia* neurons. Neuron *8*, 883–889.

Letourneau, P.C., Kater, S.B., and Macagno, E.R. (eds.) (1991). The Nerve Growth Cone, New York: Raven Press.

Lewis, A.K., and Bridgman, P.C. (1992). Nerve growth cone lamellipodia contain two populations of actin filaments that differ in organization and polarity. J. Cell Biol. *119*, 1219–1243.

Lin, C.H., Espreafico, E.M., Mooseker, M.S., and Forscher, P. (1996). Myosin drives retrograde f-actin flow in neural growth cone. Neuron *16*, 769–782.

Lin, C.H., and Forscher, P. (1993). Cytoskeletal remodeling during growth cone-target interactions. J. Cell Biol. *121*, 1369–1383.

Lin, C.H., and Forscher, P. (1995). Growth cone advance is inversely proportional to retrograde f-actin flow. Neuron *14*, 763–771.

Maeda, Y. (1978). Birefringence of oriented thin filaments in the I-bands of crab striated muscle and comparison with the flow birefringence of reconstituted thin filaments. Eur. J. Biochem. *90*, 113–121.

McCaig, C.D. (ed.) (1996). Nerve Growth and Guidance, London: Portland Press.

Mitchison, T., and Kirschner, M. (1988). Cytoskeletal dynamics and nerve growth. Neuron *1*, 761–772.

Mitchison, T.J., and Cramer, L.P. (1996). Actin-based cell motility and cell locomotion. Cell *84*, 371–379.

Okabe, S., and Hirokawa, N. (1991). Actin dynamics in growth cones. J. Neurosci. *11*, 1918–1929.

Oldenbourg, R. (1991). Analysis of edge birefringence. Biophys. J. *60*, 629–641.

Oldenbourg, R. (1996). A new view on polarization microscopy. Nature *381*, 811–812.

Oldenbourg, R. (1999). Polarized light microscopy of spindles. In: Methods in Cell Biology; Structure, Composition and Function of the Mitotic/Meiotic Spindle, ed. C. Rieder, London: Academic Press.

Oldenbourg, R., and Mei, G. (1995). New polarized light microscope with precision universal compensator. J. Microsc. *180*, 140–147.

Oldenbourg, R., Salmon, E.D., and Tran, P.T. (1998). Birefringence of single and bundled microtubules. Biophys. J. *74*, 645–654.

Ramon y Cajal, S. (1909). Histologie du système nerveux de l'homme et des vertébrés, Paris: Maloine.

Ramon y Cajal, S. (1995). Histology of the Nervous System of Man and Vertebrates, New York: Oxford University Press.

Rochlin, M.W., Dailey, M.E., and Bridgman, P.C. (1997). Intrapodia: novel, actin-rich structures that advance through nerve growth cone lamellipodia. Mol. Biol. Cell *8*, 256a.

Salmon, E.D. (1975). Pressure-induced depolymerization of spindle microtubules. I. Spindle birefringence and length changes. J. Cell Biol. *65*, 603–614.

Sanger, J.M., Sanger, J.W., and Southwick, F.S. (1992). Host cell actin assembly is necessary and likely to provide the propulsive force for intracellular movement of *Listeria monocytogenes*. Infect. Immun. *60*, 3609–3619.

Sato, H., Ellis, G.W., and Inoué, S. (1975). Microtubular origin of mitotic spindle form birefringence demonstration of the applicability of Wiener's equation. J. Cell Biol. *67*, 501–517.

Small, V.J. (1994). Lamellipodia architecture: actin filament turnover and the lateral flow of actin filaments during motility. Semin. Cell Biol. *5*, 157–163.

Smith, S.J. (1988). Neuronal cytomechanics: the actin-based motility of growth cone. Science *242*, 708–715.

Soranno, T., and Bell, E. (1982). Cytostructural dynamics of spreading and translocating cells. J. Cell Biol. *95*, 127–136.

Taylor, D.L. (1976). Quantitative studies on the polarization optical properties of striated muscle. I. Birefringence changes of rabbit psoas muscle in the transition from rigor to relaxed state. J. Cell Biol. *68*, 497–511.

Theriot, J.A., and Mitchison, T.J. (1991). Actin filament dynamics in locomoting cells. Nature *352*, 126–131.

Theriot, J.A., Mitchison, T.J., Tilney, L.G., and Portney, D.A. (1992). The rate of actin based motility of intercellular *Listeria monocytogenes* equals the rate of actin polymerization. Nature *357*, 257–260.

Tosney, K.W., and Wessells, N.K. (1983). Neuronal motility: the ultrastructure of veils and microspikes correlates with their motile activities. J. Cell Sci. *61*, 389–411.

Tran, P., Salmon, E.D., and Oldenbourg, R. (1995). Quantifying single and bundled microtubules with the polarized light microscope. Biol. Bull. *189*, 206.

Wang, F.S., Wolenski, J.S., Cheney, R.E., Mooseker, M.S., and Jay, D.G. (1996). Function of myosin-V in filopodial extension of neuronal growth cones. Science *273*, 660–663.

Wang, Y.L. (1985). Exchange of actin subunits at the leading edge of living fibroblasts: possible role of treadmilling. J. Cell Biol. *101*, 597–602.

Welch, M.D., Mallavarapu, A., Rosenblatt, J., and Mitchison, T.J. (1997). Actin dynamics *in vivo*. Curr. Opin. Cell Biol. *9*, 54–61.

Welnhofer, E.A., Zhao, L., and Cohan, I. (1997). Actin dynamics and organization during growth cone morphogenesis in Helisoma neurons. Cell Motil. Cytoskeleton *37*, 54–71.

Yamada, K.M., Spooner, B.S., and Wessells, N.K. (1971). Ultrastructure and function of growth cones and axons of cultured nerve cells. J. Cell Biol. *49*, 614–635.

Yamada, K.M., Spooner, B.S., and Wessells, N.K. (1970). Axon growth: role of microfilaments and microtubules. Proc. Natl. Acad. Sci. USA *66*, 1206–1212.